Agent-based Social Simulation of Spatiotemporal Process-triggered Graph Dynamical Systems - Technical Report

Zakaria Mehrab[1,2] S. S. Ravi[2] Henning Mortveit[2,3] Srinivasan Venkatramanan[2]
Samarth Swarup[2] Bryan Lewis[2] David Leblang[4]
Madhav Marathe[1,2]

[1]Dept. of Computer Science, University of Virginia, VA, USA
[2]Biocomplexity Institute, University of Virginia, VA, USA
[3]Department of Systems and Information Engineering, University of Virginia, VA, USA
[4]Department of Politics and Batten School of Public Policy, University of Virginia, VA, USA

June 27, 2025

ABSTRACT

Graph dynamical systems (GDSs) are widely used to model and simulate realistic multi-agent social dynamics, including societal unrest. This involves representing the multiagent system as a network and assigning functions to each vertex describing how they update their states based on the neighborhood states. However, in many contexts, social dynamics are triggered by external processes, which can affect the state transitions of agents. The classical GDS formalism does not incorporate such processes. We introduce the *STP-GDS* framework, that allows a GDS to be triggered by spatiotemporal background processes. We present a rigorous definition of the framework followed by formal analysis to estimate the size of the active neighborhood under two types of process distribution. The real-life applicability of the framework is further highlighted by an additional case study involving evacuation due to natural events, where we analyze collective agent behaviors under heterogeneous environmental and spatial settings.

1 Introduction

Graph Dynamical Systems (GDSs) are used to simulate dynamics of networked multiagent systems across many fields such as epidemiology, biology, and sociology (see e.g., [1, 2, 3, 4, 5]). An informal description of a GDS is provided here. In a GDS, the population is represented as a network, where vertices denote agents and edges denote interactions among agents. Each vertex can assume state values from a predefined domain, which is usually finite (e.g., $\{0,1\}$). Each vertex v is assigned a vertex-local function that considers the current state of v and those of its neighbors to calculate the next state of v. An update scheme (e.g., synchronous update, sequential update using a permutation of the vertices) determines the order in which the vertices compute and update their states. Various questions regarding network dynamics, such as configuration reachability [6, 7, 8], fixed point existence [9, 10], and predecessor existence [11] have been studied both analytically and empirically[1]. An extensive body of work has extended the classical GDS formalism in

[1]The *configuration reachability* problem involves determining whether a GDS can reach a given configuration starting at a specified initial configuration. A *fixed point* of a GDS is a configuration from which the GDS doesn't change to another configuration.

various directions. We will discuss the relevant extensions in Section 2 ("Related Work").

However, when one considers the study of networked multi-agent system dynamics using GDSs in the context of social unrest, there is a gap in the classical formalism and its extensions. External background processes often trigger social unrest. Forced migration due to conflict events is one such situation. We previously attempted to study such dynamics by considering both the effect of events and peer influence [12, 13]. However, since these studies did not use a formal framework, there was little scope for a systematic analysis.

To address this gap, we make the following contributions in this paper. *First,* we propose the novel framework of a **S**patio**T**emporal **P**rocess Triggered **G**raph **D**ynamical **S**ystem (*STP-GDS*) to model the dynamics of a networked multi-agent system that incorporates the effect of both background processes and peer influence. Motivated by our prior work on conflict-induced forced migration and the fact that real-life social unrest occurs within a geographic boundary, we consider the agents and processes explicitly in Euclidean space and develop the necessary formalism to make the framework capable of handling the interaction between agents and events (Section 3.1). *Second,* by modeling the impact of the events and agent states through a threshold model that considers both the impact of events and neighborhood states, we analytically derive a lower bound on the expected peer influence during an agent's transition point under a known process distribution (Section 3.3). During social unrest situations, when getting a complete picture of the entire population is non-trivial, such analyses can be useful to policymakers. We also empirically evaluate our analytical results with a case study (Section 4.1). *Finally*, we deploy our framework through a small case study involving evacuation due to coastal erosion, where the processes do not follow any known distribution and showcase how our framework can be utilized to study evacuation dynamics in different environmental and structural conditions (Section 4.2). This case study reveals that while the overall evacuation dynamics is sensitive to the spatial structure of the events and the agents in less event-intensive scenarios, it is less sensitive in highly event-intensive scenarios.

2 Related Work

GDS Frameworks: As mentioned earlier, the GDS model has been extended by many researchers to develop simulation systems for various applications. For example, a general GDS framework (called InterSim) where dynamics across multiple contagions can be handled is presented in [3]. This system also includes a simulation tool where users can define their own models to extend the framework and generate simulation dynamics. A system (called GDSCalc) that can compute many characteristics of GDSs (e.g., the trajectory of a system from a given initial configuration, presence/absence of fixed points) is discussed in [14]. Another work [2] introduced stochastic GDSs, where the transition functions choose the next state probabilistically rather than deterministically. Such a model and its variants are commonly used in epidemic simulations (see e.g., Adiga et al. [1] and the references cited therein). The threshold model [15] is a popular choice among the transition functions studied across various references on GDS (e.g., [16, 17]). Other extensions of the threshold model have also been proposed [18] to understand agent dynamics in various social unrest situations [19, 20].

Process Triggered ABM: Agent-based models (ABMs) and simulation approaches for studying migration due to wars have been considered by many researchers (see e.g., Biondo et al. [21], Maidanik [22], Mehrab et al. [23] and the references cited therein). Biondo et al. [21] developed a utility function based on the social network associated with a migrant to determine when the individual would return to their home country. Maidanik [22] uses a survey-based approach to model return migration from Ukraine due to the conflict with Russia. Mehrab et al. [12] use an ABM to study migration decisions resulting from the combined

A *predecessor* of a configuration C is a configuration C' such that the GDS changes from C' to C in one step.

effect of conflict events and peer influence. However, to our knowledge, a formal framework to analyze the effect of events and peer influence is absent in the literature.

3 General Framework

Table 1: Symbols and their meanings used in the paper for the proposed framework and subsequent analysis.

Threshold based STP-GDS Framework		*Analysis & Case Studies*	
Symbol	Description	Symbol	Description
$\mathbb{G}$	Augmented Agent Network	$\rho_v(t)$	Active neighborhood fraction of v at t
$G^t(V^t,E)$	Network configuration at time t	α	Distance decay parameter
$v:(x_v^t,y_v)$	Agent $v \in V^t$ action state at time t and location	θ_v	Temporal discounting rate parameter
$\mathbb{S}$	Action State Domain	r_v	Visibility radius of v
$\mathbb{B}$	Set of background processes/events	λ	Event rate parameter (Homogeneous Poisson)
(t_b,z_b)	Time and location of process $b \in \mathbb{B}$	λ_0	Base Event rate (Hawkes)
$\mathbb{O}$	Observation profile	$\lambda(t\|\mathbb{H}_t)$	Conditional event intensity at t (Hawkes)
$O_v(t,b)$	v's observation of event b at time t	$\phi(\cdot)$	Trigger function (Hawkes)
$\mathbb{F}$	Action update functions	η	Base parameter when $\phi(t)=\eta e^{-\beta t}$
f_v	Action update function of v	β	Change rate parameter when $\phi(t)=\eta e^{-\beta t}$
$\mathcal{N}_v$	Open neighborhood of v	T_E	Event generation time (Case Study 1)
$\mathbb{W}$	Update Scheme	T_S	Simulation time (Case Study 1)
H_v^t	Event impact on v at t	$WS(N,K,P)$	Watts-Strogatz Graph Model [24]
$h_{v,b}^t$	Event b's impact on v at t	$BA(N,M)$	Barabasi-Albert Graph Model [25]
K_s	Spatial Kernel Function	g	Grid subdivision parameter (Case Study 2)
K_t	Temporal Kernel Function	$\sigma(\cdot)$	Activation function
γ_1	Peer influence weight	Q	Evacuation bias for $\sigma(x)=(1+Qe^{-\omega x})^{-1}$
γ_2	Event influence weight	ω	Risk growth for $\sigma(x)=(1+Qe^{-\omega x})^{-1}$
τ_v	State transition threshold of v	N_E	Number of events (Case Study 2)

In this section, we formulate our general *STP-GDS* framework. We begin with the definitions of the basic components of the framework. Then, the definitions are extended to formulate the threshold function based *STP-GDS* to develop further analytical and empirical insights about the framework.

3.1 Definitions

An *STP-GDS* is given by the tuple ($\mathbb{G}$, $\mathbb{S}$, $\mathbb{B}$, $\mathbb{O}$, $\mathbb{F}$, $\mathbb{W}$), where:

1. The augmented agent network $\mathbb{G}$ is a set of configurations $\{G^0, G^1, G^2, \ldots, G^T\}$, where the network configuration at time t is denoted by $G^t(V^t,E)$. We assume that the set of vertices and edges remain static over time. However, the states of the vertices may change temporally. Each vertex $v \in V^t$ is associated with an action state x_v^t from the domain $\mathbb{S}$ (whose role is explained in Item 2 below). This corresponds to the action of agent v at time t. We also assume that each vertex is associated with a static state $y_v \in \mathbb{R}^\delta$, which denotes the location of v in the $\delta-$dimensional Euclidean space.
2. $\mathbb{S}$ is the domain for the agent action states. The choice of $\mathbb{S}$ depends upon the specific use-case. For example, when $\mathbb{S} \in \{0,1\}$, x_v^t can denote whether the vertex is inactive or active [18].
3. $\mathbb{B}$ is the set of spatio-temporal background processes. Each background process $b \in \mathbb{B}$ is associated with t_b, the time of the event (as defined before) and $z_b \subseteq \mathbb{R}^\delta$, which denotes the location of the process in the same Euclidean space as the agents. For example, if z_b consists of a single point, it denotes a point

process. If z_b is an ordered set of points representing the convex hull of a set of points, it can represent a process that takes place in a convex polygonal region. Instead of defining z_b in terms of a set of points, it can also be defined through constraints. For example, if we define $z_b = \{(z_1, z_2) \mid z_1 \in \mathbb{R}, z_2 \in \mathbb{R}, z_1^2 + z_2^2 \leq 1\}$, it denotes a process that consists of points inside and on a circle of unit radius in 2D Euclidean space centered at the origin. In this paper, we assume that events are unmarked point processes [26]. However, one can easily extend this to marked processes by introducing an additional scalar $w_b \in \mathbb{R}^+$. (In our case, $w_b = 1$ for all $b \in \mathbb{B}$.)

4. $\mathbb{O}$ is the set of observation profiles $\{O_1, O_2, ..., O_N\}$ where O_v is a binary matrix of size $T \times |\mathbb{B}|$ with $O_v(t,b) = 1(0)$ indicating whether agent v can (cannot) observe the process b at time t. Different possibilities exist on how one can specify observation profiles. For example, one can assume that at time t, agent v can observe events happening at that time within a visibility radius r_v. Let $\Delta(y_v, z_b)$ be the minimum Euclidean distance between agent v and event b. Then, one definition of the observation profile can be $O_v(t,b) = (\Delta(y_v, z_b) \leq r_v)$ AND $(t_b == t)$, where AND is the Boolean connective.
5. $\mathbb{F}$ is the collection of action update functions, where $f_v \in \mathbb{F}$ is the action update function for vertex v that takes the state of vertex v, the states of its neighbors and its observation profile O_v as inputs and produces the next state of v as output. Let $\mathscr{N}_v = \{u : (v,u) \in E\}$ denote the open neighborhood of v induced by G. Since the edge set E is assumed to be fixed along graph snapshots, $\mathscr{N}_v$ is also static. Given this, the next action state of v is given by $f_v : \mathbb{S} \times \mathbb{R}^\delta \times \mathbb{P}(\mathbb{S}) \times \mathbb{P}(\mathbb{R}^\delta) \times \mathbb{O} \to \mathbb{S}$; that is, $f_v(x_v^t, y_v, \{x_u^t\}_{u \in \mathscr{N}_v}, \{y_u\}_{u \in \mathscr{N}_v}, O_v) = x_v^{t+1}$. Here, $\mathbb{P}(Y)$ denotes the power set of Y.
6. $\mathbb{W}$ is an update scheme for the $\mathbb{F}$, which denotes the local function execution order of the vertices. For example, in a synchronous dynamical system, all vertices compute their local functions in parallel. Other update schemes, such as sequential update, block synchronous update [14], have also been studied. In our framework, we employ the synchronous update scheme, since it is by far the most explored one in literature [1].

We assume hereafter that $\mathbb{S} = \{0, 1\}$. Thus, the agents in the system can either be in inactive (0) or active (1) state. We also assume that all agents are initially inactive and the system is *progressive*; that is, once an agent transitions to the active state, it stays in that state.

3.2 Threshold function based Framework

To develop insights about the framework, we need to choose reasonable specifications for f_v, the action update function for each agent v. Here, we choose the threshold function, a popular choice in literature as the action update function of GDS [1]. Classically, in a threshold-based action update function, a vertex v goes through a state transition when the number of neighbors in a different state exceeds a specified threshold τ_v. For threshold-based *STP-GDS*, it is reasonable to assume that this threshold should be compared not only with the neighbors but also with some measure of the impact from the events, since the external influence from the processes can be sufficient for the vertices to undergo a state transition even without peer influence. Let us denote the total impact of events on agent v at time t by H_v^t. Then, we can express f_v as follows.

$$f_v : x_v^{t+1} = \begin{cases} 1 & \text{if } x_v^t = 1 \\ 1 & \text{if } \gamma_1 \sum_{u \in \mathscr{N}_v} x_u^t + \gamma_2 H_v^t \geq \tau_v \\ 0 & \text{otherwise.} \end{cases} \tag{1}$$

Here, γ_1 and γ_2 are constants that control the weight of peer influence and event influence respectively. The remaining work is to model H_v^t. Let us first model the impact of a single event b on agent v at time t, denoted by $h_{v,b}^t$. Designed by Brunsdon et al. [27], the spatiotemporal kernel density estimator (STKDE) has initially been used for event density estimation. Later, this has also been used for visualizing crime patterns [28] and predictive crime modeling [29]. We extend the STKDE formulation to assess event impact on an agent as

$h^t_{v,b} = K_s(y_v, z_b)K_t(v,t,t_b)$. Here, K_s is a kernel function for the spatial domain, and K_t is a kernel function for the temporal domain. Thus, the total impact H^t_v can be simply expressed as $H^t_v = \sum_{b\in\mathbb{B}} h^t_{v,b} O_v(t,b)$.

Depending on the choice of the kernel functions, H^t_v can assume different forms. Here, we discuss some possible choices of them. For the choice of the spatial kernel K_s, one can assume that events farther away from the agents have less impact than events nearby. Thus, one can assume $K_s(y_v, z_b) = k_s(\Delta(y_v, z_b))$ where $k_s(\cdot)$ is a decay function based on distance (e.g., exponential decay model, $k_s(d) = e^{-\alpha d}$ or gravity model, $k_s(d) = d^{-\alpha}$). For the temporal kernel K_t, one possible choice is the temporal component of the discounting utility model. Exponential discounting function is a well-studied example, and this gives K_t the following form $K_t(v,t,t_b) = \theta_v^{t-t_b}$ where θ_v $(0 \leq \theta_v \leq 1)$ is the discounting rate parameter that controls how much influence past events exert on agent v at time t. Note that, when $\theta_v = 0$, $h^t_{v,b} = 0$ unless $t = t_b$; this is an example of a *memoryless* [2] agent. When $\theta_v > 0$, the agent is *retentive*.

3.3 Analysis of Threshold Function based *STP-GDS*

Upon deciding a specific choice of the observation profile $\mathbb{O}$, the spatial kernel K_s and the temporal kernel K_t, we can study various important properties of *STP-GDS*s. In this section, we mathematically analyze one such property which we term *active neighborhood inference*. Specifically, we ask the following question: *given an agent v with degree d_v has transitioned from inactive to active state at time t, what fraction of its neighbors were already in active state?* Answering such a question can be important in scenarios with limited information. An example of such a scenario is the case of conflict-induced forced migration, when the available data regarding forced migrants is sparse. One de facto way of data collection is to perform a Random-Digit-Dial (RDD) on a sample population [32] and perform an upscale estimation. In such a case, *active neighborhood inference* can offer a principled way to approximate neighborhood state information than simple upscale approximation, assuming that state transitions occurred following a threshold-function based approach.

Suppose an agent v has $d_v \geq 1$ neighbors. If $x^{t+1}_v = 1$ and $x^t_v = 0$, and $\rho_v(t)$ is the fraction of neighbors of agent v in state 1 at time t, it follows that the following condition was satisfied at time t:

$$\gamma_1 \rho_v(t) d_v + \gamma_2 H^t_v \geq \tau_v \implies \mathbb{E}[\rho_v(t)] \geq \frac{\tau_v - \gamma_2 \mathbb{E}[H^t_v]}{\gamma_1 d_v} \tag{2}$$

where $\rho_v(t)$ and H^t_v are random variables since the external processes are regarded as random events. To calculate $\mathbb{E}[H^t_v]$, we begin by making specific assumptions about the distribution of the process. Moreover, we consider the space of the agents and the events to be the 2D Euclidean space, since the case studies we conduct are based on real-life process-based events that happen in 2D geographic space.

Poisson Process Distribution: For this analysis, we assume that the events can happen uniformly anywhere within the circle of radius r from v's perspective and they are Poisson-distributed with a mean of λ temporally. Accordingly, we assume the observation profile for v as $O_v(t,b) = (\Delta(y_v, z_b) \leq r_v)$ AND $(t_b \leq t)$, $K_t(v,t,t_b) = \theta_v^{t-t_b}$ and $K_s(y_v, z_b) = k_s(\Delta(y_v, z_b))$. Then, the following result can be shown.

Proposition 1. *In a threshold-based* STP-GDS *with decay based spatial kernel and exponential discounting temporal kernel (parameterized by θ_v), if events are Poisson distributed with rate λ with respect to an agent v with visibility radius r_v, then the expected impact from events at time t on agent v can be expressed as: $\mathbb{E}[H^t_v] = \lambda \frac{1-\theta_v^t}{1-\theta_v} \int_0^{r_v} k_s(x) \frac{2x}{r_v^2} dx$, where x is the random variable corresponding to the minimum distance between the event and the agent.*

[2] We adopt the convention of setting $\theta_v^{t-t_b} = 1$ when $\theta_v = 0$ and $t = t_b$, to ensure that only the current reward is preserved, consistent with choices made for expansion of power series. See [30] and [31] for relevant discussions.

A detailed derivation is provided in the Appendix B. Depending on the choice of $k_s(x)$, a closed-form of the above expression can be derived. One such example is when the exponential decay model $k_s(x) = e^{-\alpha x}$ is considered. In such a case, the following result holds.

Corollary 1.1. *For exponential decay spatial kernel $k_s(x) = e^{-\alpha x}$ and the setting outlined in Proposition 1, the expected fraction of active neighborhood satisfies the following lower bound:*

$$\mathbb{E}[\rho_v(t)] \geq \frac{(1-\theta_v)\alpha^2 r_v^2 \tau_v - 2\gamma_2\lambda(1-\theta_v^t)(1-e^{-\alpha r_v}(1+\alpha r_v))}{(1-\theta_v)\alpha^2 r_v^2 \gamma_1 d_v} \tag{3}$$

Proof: To show this, we start with the observation that when $k_s(x) = e^{-\alpha x}$, the integration term for $\mathbb{E}[H_v^t]$ derived in Proposition 1 yields $\frac{2(1-e^{-\alpha r_v}(1+\alpha r_v))}{\alpha^2 r_v^2}$. Substituting the resultant $\mathbb{E}[H_v^t]$ with this expression in Equation (2) gives us the result. □

This gives us an expression for estimating number of active neighbors of an agent in a threshold-based *STP-GDS*, assuming the events are Poisson distributed with temporal rate λ and the quantities on the right hand side of this expression are known. Most of the quantities refer to the vertex v-specific attributes and can be obtained by probing the vertex v. Quantities such as $\alpha, \gamma_1, \gamma_2$ can be chosen based on historical data or empirical observations.

An interesting approximation can be obtained when the quantity αr_v is small and the agent v is memoryless. In such case, we can show the following.

Corollary 1.2. *For the exponential decay spatial kernel $k_s(x) = e^{-\alpha x}$ such that αr_v is small, agent v us memoryless (i.e., $\theta_v = 0$), and the setting outlined in Proposition 1, the expected fraction of active neighborhood satisfies the following lower bound: $\mathbb{E}[\rho_v(t)] \geq \frac{\tau_v - 2\gamma_2\lambda}{\gamma_1 d_v}$.*

Our proof is in the Appendix C. It shows that, when αr_v is small, the spatial kernel does not contribute to the estimate on active neighborhood.

Hawkes Process Distribution: Across various scenarios, the events often exhibit clustering or triggering behavior; that is, events at future timesteps are often triggered by past events [26]. Such events are often characterized through the Self-exciting Hawkes process models [33]. Fundamentally, the conditional intensity of the model at time t is defined as $\lambda(t \mid \mathbb{H}_t) = \lambda_0 + \int_0^t \phi(t-u)\mathrm{d}N(u)$. Here, $\mathbb{H}_t$ is the history of past events, λ_0 is a constant background rate of events, $N(\cdot)$ is a counting measure that measures the number of events that happened at any time and $\phi(\cdot)$ is the triggering function that determines the form of *self-excitation*. Following the definition in Lesage et al. [34] where the expectation of the conditional intensity is written as $\mathbb{E}[\lambda(t)] = \lambda_0 + \int_0^t \phi(t-u)\mathbb{E}[\lambda(u)]\mathrm{d}u$, we can derive closed-form expressions for $\mathbb{E}[H_v^t]$ for various choices of $\phi(\cdot)$ and plug it into Equation (2) to derive the expected active fraction during transition point. We perform a derivation for $\mathbb{E}[H_v^t]$ for one such case.

Note that $\lambda(t)$ and λ_0 have similar context in the case of the Hawkes model as the λ in the Poisson model. However, contrary to Poisson, it is important to note that the event rate in Hawkes is time-dependent, which necessitates the use of a temporal component.

Proposition 2. *In a threshold-based* STP-GDS *with memoryless agents and exponential decay based spatial kernel ($k_s(x) = e^{-\alpha x}$), if events follow a Hawkes distribution with base intensity λ_0 and exponential triggering function $\phi(t) = \eta e^{-\beta t}$ with respect to an agent v with visibility radius r_v, then the expected impact from events at time t on agent v can be expressed as:*

$$\mathbb{E}[H_v^t] = \frac{2\lambda_0}{\alpha^2 r_v^2}\left(1 + \frac{\eta}{\beta-\eta}\left(1 - e^{-t(\beta-\eta)}\right)\right)(1 - e^{-\alpha r_v}(1+\alpha r_v)) \tag{4}$$

A proof is provided in the Appendix D. This expression can be used to obtain an approximation for the neighborhood state of a transitioning agent in a Hawkes process setting, similar to the equation derived for

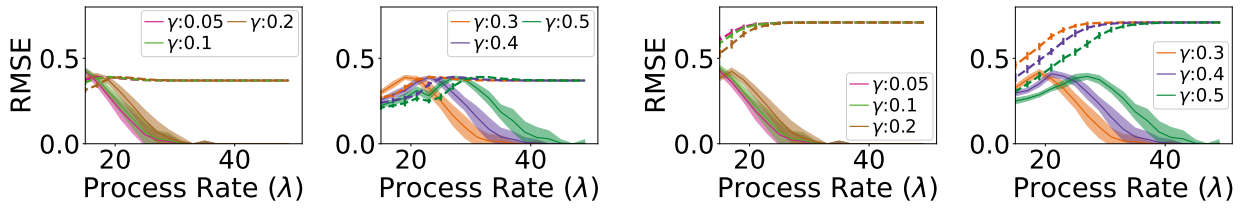

(a) $WS(N = 100, K = 30, P = 0.2)$ **(b)** $BA(N = 100, M = 11)$

Figure 1: Active neighborhood inference for threshold-based *STP-GDS* triggered by homogeneous Poisson process. The RMSE between actual fraction of active neighborhood is compared with the expected active neighborhood of our analysis (Equation (3) for agent networks modeled with WS (Figure 1a) and BA (Figure 1b). Solid lines represent our estimation with one standard deviation accounted for in the shaded region, while the dashed line represents naive estimation (τ/d_v). The estimation is shown for different rates of the process (λ) and different γ values. For a fixed rate, while our estimation deviates from the ground truth with increasing γ (more peer influence), it is always better than naive estimation when λ is high (event-intensive situation). Each experiment was repeated 50 times.

Poisson setting (Equation (3)), which can be further simplified if we choose the parameters so that $\beta - \eta$ and αr are small. In such a case, the expected fraction of active neighbors satisfies the following lower bound: $\mathbb{E}[\rho_v(t)] \geq \tau_v - 2\gamma_2\lambda_0(1+\eta t)/\gamma_1 d_v$. This suggests that, on average, agents of a *STP-GDS* where events follow Hawkes setting eventually transition to state 1 in the long run (i.e., as $t \to \infty$).

4 Case Studies

In this section, we assess the efficacy of our proposed framework by conducting two case studies. *First,* we experimentally evaluate the correctness of our active neighborhood state inference analysis by simulating networked agents forming a threshold-based *STP-GDS* with homogeneous Poisson processes in the background. Initially triggered by the events, the agents in the system change their states when the influence from the events and their peers exceeds a threshold. We show that our method better aligns with the simulation results since they incorporate information about the background spatial processes. *Second,* we apply our framework in a more realistic setting of evacuation due to coastal inundation where agents are placed in a circular island where erosion events are experienced at the periphery of the island randomly. A simulation of this system underscores how our framework can be used to explore collective agent behavior under heterogeneous settings. All simulation scripts are written in Python 3.13 and publicly available in an online GitHub repository (See Code Availability Section).

4.1 Case Study 1: Active Neighborhood State Inference

This study begins by sampling an agent network $G_{N,\Theta}$, where N is the number of agents in the environment and Θ denotes other parameters associated with the graph sampling process. For example, if we generate ER [35] networks, then $G_{N,\Theta} \approx G_{N,P}$, where P denotes the wiring probability of an edge in the ER Random Graph model. We select a homogeneous visibility radius and threshold across all agents ($r_v = r, \tau_v = \tau, \forall v$) to reduce the complexity associated with possible covariates, although we emphasize that the method works with heterogeneous values of the parameters. We also assume that $\gamma_1 + \gamma_2 = 1$, so that the total amount of influence one can allot to peer and events is fixed and only γ_1 (denoted by γ from here on) needs to be varied. Then, $\forall t \in \{1, 2, .., T_E\}$, we sample point processes around each agent within a visibility radius of r. We generate events following a homogeneous Poisson process with rate λ. Afterwards, the system is simulated for T_S steps following Equation (1) for T_S simulation steps. When agents are retentive, they may update their states after the occurrence of the last event. Therefore, it is important that $T_S > T_E$ to account for any

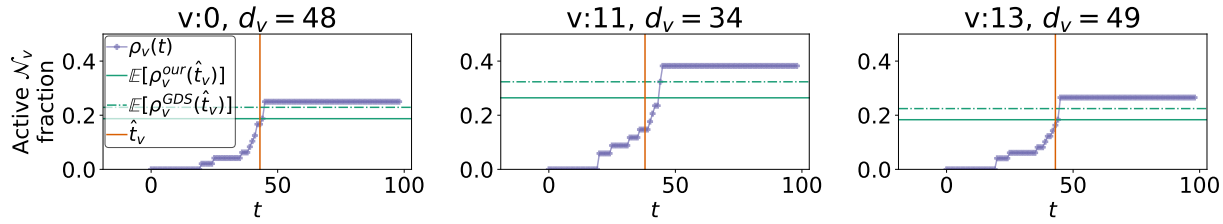

Figure 2: Dynamics of 3 active agents at the end of the simulation with $G(N = 100, M = 11)$ BA agent network model, $\lambda = 16$, and $\gamma = 0.6$. Here, we explain the dynamics for agents v_0 and v_{13}. They have similar degree and the lower bound given by Equation (3) for the fraction of neighbors in active state before these agents transition to active state are 0.187 and 0.183, respectively. On the other hand, when background processes are not taken into account, the naive estimation leads to the lower bounds of 0.23 and 0.22 respectively for those two agents. During simulation, we find that v_0 (v_{13}) transitions to active state after 0.17 (0.16) fraction of neighbors are in active state, closer to the approximation that derived from our framework. A similar argument holds for Agent v_{11}.

boundary effects. We also follow this for generality in this experiment, even though the agents are assumed to be memoryless. Initially, all agents begin at an inactive (0) state. Across all experiments, we keep the values of the following parameters invariant: $r = 1, \alpha = 0.2, \tau = 11, T_E = 45, T_S = 100$.

Once the simulation is complete, we compute the fraction of $\mathcal{N}_v$ in active state for an agent v when it undergoes a state transition. Let $\rho_v(t)$ be the fraction of active neighbors of v at time t during simulation. Let $\hat{t}_v$ denote the last timestep when agent v is inactive. We calculate $\mathbb{E}[\rho_v^{our}(\hat{t}_v)]$ using Equation (3) and compare it against $\frac{\tau}{d_v}$, denoted as $\mathbb{E}[\rho_v^{GDS}(\hat{t}_v)]$, which naively calculates the active neighborhood fraction without incorporating knowledge about background events. Finally, we compare the root mean square error (RMSE) between $\rho_v(\hat{t}_v)$ and $\mathbb{E}[\rho_v^{our}(\hat{t}_v)]$ against the RMSE between $\rho_v(\hat{t}_v)$ and $\mathbb{E}[\rho_v^{GDS}(\hat{t}_v)]$ and show it in Figure 1 across agent networks created using Watts-Strogatz (WS) [24] (Figure 1a) and Barabasi-Albert (BA) graph models [25] (Figure 1b).

First, for WS agent networks, it is apparent that our method is more suitable when the impact from events is significant (i.e., lower γ and higher λ) in dictating agents' decisions. On the other hand, for higher values of γ, there is a certain threshold for λ until which our estimation is slightly worse than the naive approximation; this is due to the stochasticity of the event generation process itself. However, once that threshold is crossed, our estimation always prevails over the naive estimation, which generates a somewhat constant RMSE due to the homogeneous degree distribution of the WS model.

Second, for BA model, which is suitable for modeling real-world networks due to its scale-free nature and power-law degree distribution, we find that our analytical estimation is always better, regardless of the values of γ. To examine this further, we observe the dynamics of one sample experiment with BA model more carefully when $\lambda = 16$ and $\gamma = 0.6$. The experiment converges with 18 out of the 100 agents reaching the active state. From the 18 active agents, we sample three of them and present their dynamics in Figure 2. The figure shows that our method was able to estimate more accurately the number of active neighborhood during the transition point of each agent compared to naive estimation.

4.2 Case Study 2: Evacuation due to Coastal Erosion

While the previous case study assumed a homogeneous Poisson rate, real-life events usually do not follow such a well-defined distribution. Moreover, the previous study focused on inferring state from the perspective of individual agents. However, it is often interesting to study the behavior of such a system as a collective. In this section, we demonstrate how the *STP-GDS* framework can be used to study the collective behavior of agents in a situation motivated by real-world events. Specifically, we create a small environment where people are living on a circular island which is faced with coastal erosion due to sea level rise and other

climate-related factors. Each coastal erosion event is represented as a point process along the circumference of the island. In this situation, the inhabitants may choose to stay on the island or decide to evacuate. Such analysis has real-life importance since evacuation due to coastal erosion has been studied in the context of different regions [36, 37, 38].

Modeling under *STP-GDS*: We express the model dynamics using our *STP-GDS* framework as follows. ***First*** ***(***$\mathbb{G}$***)***, for a configuration $G^t(V^t, E) \in \mathbb{G}$, each vertex $v \in V^t$ is associated with: the decision variable $x_v^t \in \mathbb{S}$, and the location variable $y_v \in \mathbb{R}^2$. The locations are points on the 2D Euclidean plane and are assumed to be stationary (household location). ***Second*** ***(***$\mathbb{S}$***)***, we assume that the decision variable is binary, where $x_v^t = 1$ ($x_v^t = 0$) means that agent v has decided to evacuate (not evacuate) by time t. Thus, $\mathbb{S} = \{0, 1\}$. ***Third*** ***(***$\mathbb{B}$***)***, each background process $b \in \mathbb{B}$ is assumed to be an unmarked point process with unit weight representing a coastal erosion event and associated with location $z_b \in \mathbb{R}^2$ and time t_b of the erosion. ***Fourth*** ***(***$\mathbb{O}$***)***, we allow the agents to have a large visibility radius; they can observe all current and past events. Thus, $O_v(t, b) = t_b \leq t$. ***Fifth***$(\mathbb{F})$, we use a threshold function as defined in Equation (1) with two modifications in the second condition. Instead of the total number of neighbors, we look at the normalized neighbors and instead of using H_v^t as the event influence, we use $\sigma(H_v^t)$ as the event influence, where σ is the activation function of the form $\sigma(x) = (1 + Qe^{-\omega x})^{-1}$, a simple parameterization of the general logistic equation, that transforms the value of H_v^t to a value between 0 and 1. Here Q and ω are parameters to control the initial bias and growth rate of the activation function, respectively. This modification allows us to control the bounds of the threshold parameter. Consequently, the second condition in the update rule of Equation (1) has the form 1 if $\gamma \frac{\sum_{u \in \mathcal{N}_v} x_u^t}{d_v} + \sigma(H_v^t)(1 - \gamma) \geq \tau$. ***Finally*** $(\mathbb{W})$, we assume the update scheme is synchronous.

Environment: Events are sampled along the circumference of a circle of radius R, representing the island. The agents are placed around the centroid in a subgrid-like structure, a structure used for representing actual population [39]. A parameter g, used to control the number of grid subdivision of the circle-inscribed square, controls the placement of the agents. Figure 3 shows some possible placements of agents and the events. The edges of the network were sampled based on ER random graph [35] model. While other network models that consider proximity (e.g., KSW [40]) exist, their multi-parametric form introduces complexity. Here, we explored the evacuation dynamics based on graph connectivity only. However, the dynamics arising from a more spatial network would certainly exhibit differences.

Simulation Settings: We simulate the evacuation dynamics of the agents across multiple settings. *First*, we generate two scenarios of coastal erosion events. In the first scenario, there are 10 events, which we refer to as the friendly environment. The other one is referred to as a hostile environment, where 50 events are generated. *Second,* agents are placed according to various grid subdivision values $g \in \{1, 2, 4, 16\}$. *Third*, the wiring probability p of the ER model is varied. *Finally*, the number of agents and the fractional threshold parameter τ are varied. We are interested in observing how the overall dynamics evolves as a result of the interactions among these covariates. To account for uncertainties associated with the location of the events, network sampling, and the locations of agents, each experiment was repeated 100 times. As for the other parameters, we fixed the following values for them: $\forall v$, $\theta_v = 0.9$, $Q = 23.3$, $\omega = 0.8$, $\alpha = 2$, $\gamma = 0.5$. A subset of the final results is shown in Figure 4 which displays the median result of the experiments with a 50% confidence interval. We highlight some key observations from the plots in Figure 4 below. Additional results can be found in our extended paper [41].

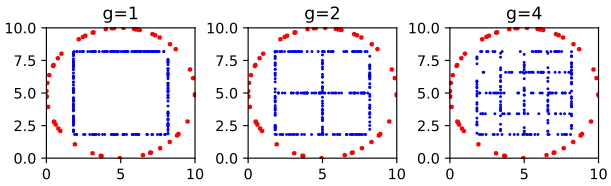

Figure 3: Environment of coastal erosion study. Red points denote erosion events along the island's border and blue dots represent agent locations.

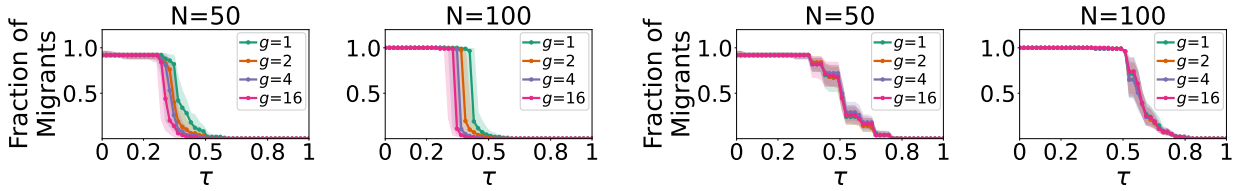

(a) Friendly ($N_E = 10$) Environment, Sparse ($p = 0.05$) Network **(b)** Hostile ($N_E = 50$) Environment, Sparse ($p = 0.05$) Network

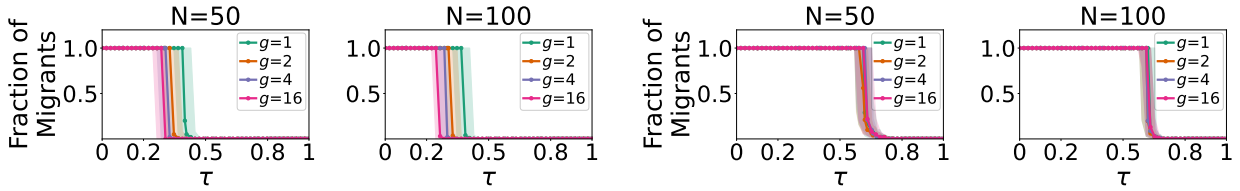

(c) Friendly ($N_E = 10$) Environment, Dense ($p = 0.3$) Network **(d)** Hostile ($N_E = 50$) Environment, Dense ($p = 0.3$) Network

Figure 4: Evacuation dynamics under different conditions. The top row figures correspond to sparse agent connectivity and bottom-row figures are for dense connectivity.

Simulation Results: Sensitivity to τ is readily observable in Figure 4. *First*, the total number of evacuees at the end of the simulation is correlated to the environment sensitivity; as τ increases, sensitivity to peers and events decreases and so does the total number of evacuees. Moreover, this correlation depicts a phase-transition-like behavior before and after certain ranges of values for τ; within a small variation in τ, the total number of evacuees drops from almost everyone to virtually nobody. *Second*, we observe that the steepness of the transition varies depending on the network structure and the environment type. The transition is more abrupt for dense networks (bottom row) than for sparse networks (top row). On the other hand, for networks with similar density, the transition is less abrupt under a hostile environment. This indicates the possibility of a dynamical system under an event-intensive environment with a large number of fixed points, possibly due to the creation of pockets of evacuees inside the network due to a wider point process distribution. This makes having diverse scenarios more probable, which attributes to the different fixed points. *Third*, the critical value of τ, where the phase transition occurs, is lower in the case of a friendly environment than in a hostile environment. This is intuitive since in an event-intensive scenario, it is possible to reach the threshold through impact from the events even when τ is very high. Thus, the switch from total evacuation to no evacuation does not happen until a very high τ (bottom right figure).

The second observation is related to the *sensitivity with respect to g*. Interestingly, across the simulations corresponding to the friendly environment, we find that the phase transition occurs for higher τ when $g = 1$ than the case of $g > 1$. The reason for this behavior can be understood by examining Figure 3. When $g = 1$, no matter on which edge an agent v is located, there is an equal likelihood that v will experience coastal erosion along the border that is closest to the edge on which v is placed. On the other hand, for $g > 1$, since agents living on the inner grid cells are closer to the center of the island, they might be far away from these events. The effect of the events is much less on the agents in the inner grid cells as they are farther away from those events compared to those on the outer grid cells. In the network, if an agent v in an outer grid cell has many neighbors who are in inner grid cells, then v may not have enough motivation to evacuate. Therefore, the phase transition occurs for a lower value of τ in the case of $g > 1$ than the case of $g = 1$. This phenomenon, however, is less prominent in a hostile environment, where the summation of the impacts of different events from different directions ultimately causes both boundary agents and central agents to behave similarly. Note that g is only responsible for affecting agent-event proximity. It does not affect agent-agent proximity due to the aspatial nature of ER. Under a spatial network model, the dynamics would

show a more prominent dependence on g.

Finally, we analyze the *sensitivity with respect to N* (the number of agents) and P (the wiring probability). The agent dynamics appear to be generally robust with respect to N, the only difference being that there seems to be a curvature along the right limit of τ where the phase transition occurs for lower N, whereas the transition is steeper for higher N. Lastly, when P is low in the case of 50 agents, for lower values of τ, some agents never evacuate, regardless of whether the environment is hostile or friendly. This is due to isolated agents that do not experience evacuation caused by low average degrees (≈ 2.45 in this case).

5 Summary and Future Work

To simulate social dynamics triggered by external events, we propose the *STP-GDS* formal framework, which provides a principled way to analyze how a networked system of agents behaves under combined influence from these events and peers. We show how this framework can be used to develop analytical insights about agent configurations for known underlying process distributions. We also demonstrate how this framework can be configured to simulate a social unrest setting by conducting a case study motivated by a real-life crisis example. Evaluating the agreement of this framework with ground truth information is a natural future direction. Moreover, this framework assumes spatially static agents. Extending this framework to incorporate mobile agents through dynamic network reconfiguration is of importance from a policymaking perspective. A comparison of this extended framework under various mobility models is a promising research direction.

ACKNOWLEDGMENTS

This work was supported in part by NSF grant #2053013, DTRA contract HDTRA1-19-D-0007, NSF grant OAC-1916805 , NSF Expeditions in Computing grant CCF-1918656, UVA Strategic Investment Fund award number SIF160, and the Strategic Investment Fund Award to the UVA's Humanitarian Collaborative.

APPENDIX

A Summary statement for important equations

B Proof for Proposition 1

Our proof uses linearity of expectation [42].

$$\mathbb{E}[H_v^t] = \mathbb{E}[\sum_{b\in\mathbb{B}} h_{v,b}^t O_v(t,b)] = \mathbb{E}[\sum_{t'=1}^{t} \sum_{b\in\mathbb{B}, t_b=t', \Delta(y_v,z_b)\le r_v} h_{v,b}^t] = \mathbb{E}[\sum_{t'=1}^{t} \sum_{b\in\mathbb{B}, t_b=t', \Delta(y_v,z_b)\le r_v} K_t(v,t,t')K_s(y_v,z_b)]$$

$$\mathbb{E}[H_v^t] = \mathbb{E}[\sum_{t'=1}^{t} \sum_{b\in\mathbb{B}, t_b=t', \Delta(y_v,z_b)\le r_v} \theta_v^{t-t'} k_s(\Delta(y_v,z_b))] = \mathbb{E}[\sum_{t'=1}^{t} \theta_v^{t-t'} \sum_{b\in\mathbb{B}, t_b=t', \Delta(y_v,z_b)\le r_v} k_s(\Delta(y_v,z_b))]$$

$$\mathbb{E}[H_v^t] = \sum_{t'=1}^{t} \theta_v^{t-t'}\lambda\ \mathbb{E}[k_s(\Delta(y_v,z_b))] = \sum_{t'=1}^{t} \theta_v^{t-t'}\lambda \int_0^{r_v} k_s(x)\frac{2x}{r^2}dx = \lambda\frac{1-\theta_v^t}{1-\theta_v}\int_0^{r_v} k_s(x)\frac{2x}{r_v^2}dx$$

C Proof for Corollary 1.2

First, when $\theta_v = 0$, Equation (3) reduces to $\mathbb{E}[\rho_v(t)] \geq \frac{\alpha^2 r_v^2 \tau_v - 2\gamma_2\lambda(1-e^{-\alpha r_v}(1+\alpha r_v))}{\alpha^2 r_v^2 \gamma_1 d_v}$. When αr_v is small, we can use Taylor series approximation up to first-order to rewrite it as $\mathbb{E}[\rho_v(t)] \geq \frac{\alpha^2 r_v^2 \tau_v - 2\gamma_2\lambda(1-e^{-\alpha r_v}(1+\alpha r_v))}{\alpha^2 r_v^2 \gamma_1 d_v} \approx \frac{\alpha^2 r_v^2 \tau_v - 2\gamma_2\lambda(1-(1-\alpha r_v)(1+\alpha r_v))}{\alpha^2 r_v^2 \gamma_1 d_v} = \frac{\alpha^2 r_v^2 \tau_v - 2\gamma_2\lambda\alpha^2 r_v^2}{\alpha^2 r_v^2 \gamma_1 d_v} = \frac{\tau_v - 2\gamma_2\lambda}{\gamma_1 d_v}$.

D Proof for Proposition 2

By letting $\mathbb{E}[\lambda(t)] - \lambda_0 = v(t)$, we can write $\mathbb{E}[\lambda(t)] = \lambda_0 + \int_0^t \phi(t-u)\mathbb{E}[\lambda(u)]\mathrm{d}u$ instead as $v(t) = \int_0^t \phi(t-u)v(u)\mathrm{d}u + \lambda_0 \int_0^t \phi(t-u)\mathrm{d}u$. Applying Laplace transform on this equation, we obtain:

$$\mathscr{L}[v(t)] = \mathscr{L}\left[\int_0^t \phi(t-u)v(u)\mathrm{d}u\right] + \mathscr{L}\left[\lambda_0 \int_0^t \phi(t-u)\mathrm{d}u\right] \quad = \mathscr{L}[v(t) \circledast \phi(t)] + \lambda_0 \mathscr{L}\left[\int_0^t \phi(t-u)\mathrm{d}u\right]$$

One common trigger function assumes the exponent nature [43] ($\phi(t) = \eta e^{-\beta t}$). Since, $\mathscr{L}[\eta e^{-\beta t}] = \frac{\eta}{\beta+s}$, where s is the domain of Laplace Transform, we have the following.

$$\begin{aligned}
\mathscr{L}[v(t)] = \mathscr{L}[v(t)]\frac{\eta}{\beta+s} + \lambda_0 \mathscr{L}\left[\int_0^t \eta e^{-\beta(t-u)}\mathrm{d}u\right] \quad &= \mathscr{L}[v(t)]\frac{\eta}{\beta+s} + \frac{\eta\lambda_0}{\beta}\mathscr{L}\left[1-e^{-\beta t}\right] \\
\implies \mathscr{L}[v(t)] = \frac{\eta\lambda_0}{\beta}\mathscr{L}\left[1-e^{-\beta t}\right] / \left(1-\frac{\eta}{\beta+s}\right) \quad &= \frac{\eta\lambda_0}{\beta}\left(\frac{1}{s} - \frac{1}{\beta+s}\right) / \left(1-\frac{\eta}{\beta+s}\right) = \frac{\eta\lambda_0}{s(\beta+s-\eta)}
\end{aligned}$$

From here, we can start applying inverse Laplace transform to obtain our intended expectation

$$\begin{aligned}
\mathscr{L}[\mathbb{E}[\lambda(t)] - \lambda_0] = \frac{\eta\lambda_0}{s(\beta+s-\eta)} \implies \mathscr{L}[\mathbb{E}[\lambda(t)]] &= \frac{\lambda_0}{s} + \frac{\eta\lambda_0}{s(\beta+s-\eta)} \\
\implies \mathbb{E}[\lambda(t)] = \mathscr{L}^{-1}\left[\frac{\lambda_0}{s}\right] + \frac{\eta\lambda_0}{\beta-\eta}\mathscr{L}^{-1}\left[\frac{1}{s} - \frac{1}{\beta+s-\eta}\right] &= \lambda_0 + \frac{\eta\lambda_0}{\beta-\eta}\left(1-e^{-t(\beta-\eta)}\right)
\end{aligned}$$

Similar to Proposition 1, here we again assume uniform spatial distribution of the events within the visibility radius r_v from perspective of agent v, expoential spatial kernel ($(k_s(x) = e^{-\alpha x})$) and derive the expression for $\mathbb{E}[H_v^t]$. However, instead of a constant expected λ number of events, we replace that quantity by $\lambda_0 + \frac{\eta\lambda_0}{\beta-\eta}\left(1-e^{-t(\beta-\eta)}\right)$ and get the following expression for $\mathbb{E}[H_v^t]$ to complete the proof.

$$\mathbb{E}[H_v^t] = \left(\lambda_0 + \frac{\eta\lambda_0}{\beta-\eta}\left(1-e^{-t(\beta-\eta)}\right)\right)\frac{1-\theta_v^t}{1-\theta_v}\int_0^{r_v} e^{-\alpha x}\frac{2x}{r_v^2}dx = \frac{2\lambda_0}{\alpha^2 r_v^2}\left(1 + \frac{\eta}{\beta-\eta}\left(1-e^{-t(\beta-\eta)}\right)\right)(1-e^{-\alpha r_v}(1+\alpha r_v))$$

Here, the term $\frac{1-\theta_v^t}{1-\theta_v}$ was ommitted assuming memoryless agents.

E Additional Experimental Results

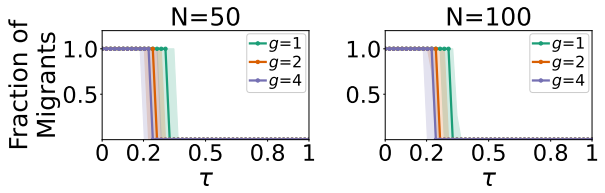

(a) Friendly ($N_E = 10$) Environment, Very Dense ($p = 0.9$) Network

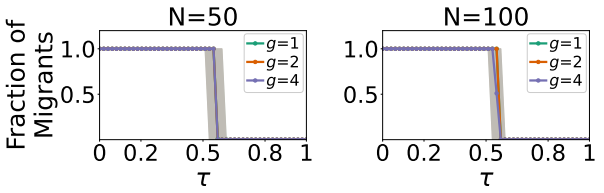

(b) Hostile ($N_E = 50$) Environment, Very Dense ($p = 0.9$) Network

Figure 5: Evacuation dynamics in very dense agent network.

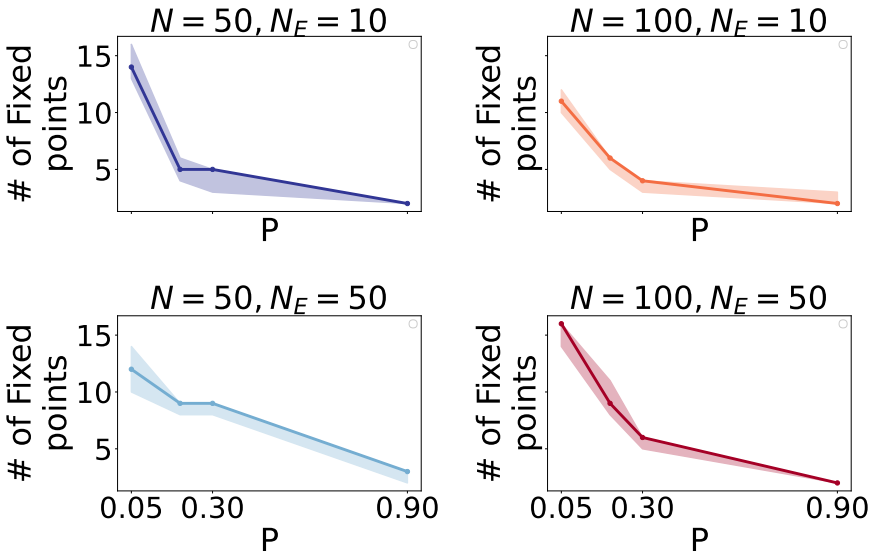

Figure 6: Fixed Points

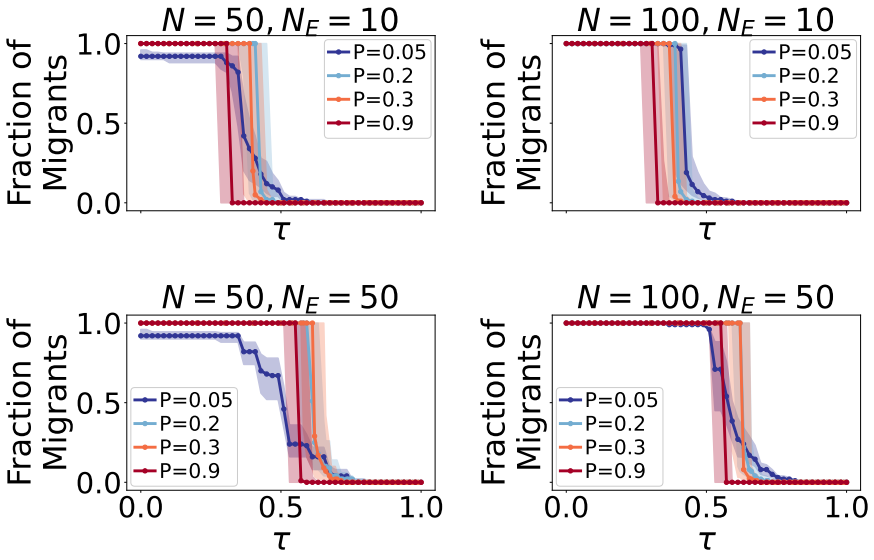

Figure 7: Dynamics under various connectivity

References

[1] A. Adiga *et al.*, "Graphical dynamical systems and their applications to bio-social systems," *International Journal of Advances in Engineering Sciences and Applied Mathematics*, vol. 11, pp. 153–171, 2019. 1, 2, 4

[2] C. L. Barrett *et al.*, "Modeling and analyzing social network dynamics using stochastic discrete graphical dynamical systems," *Theor. Comput. Sci.*, vol. 412, no. 30, pp. 3932–3946, 2011. 1, 2

[3] C. J. Kuhlman *et al.*, "A general-purpose graph dynamical system modeling framework," in *Proc. of WSC 2011*. New York, NY: IEEE, 2011, pp. 296–308. 1, 2

[4] M. Hancock *et al.*, "Data-driven modeling of evacuation decision-making in extreme weather events," in *Proc. of the COMPLEX NETWORKS 2021 10*. Springer, 2022, pp. 681–692. 1

[5] S. E. Abdelhamid *et al.*, "Agent-based modeling and simulation of depression and its impact on student success and academic retention," in *2016 ASEE Annual Conference & Exposition*, 2016, pp. 1–20. 1

[6] C. L. Barrett *et al.*, "Complexity of reachability problems for finite discrete dynamical systems," *Journal of Computer and System Sciences*, vol. 72, no. 8, pp. 1317–1345, 2006. 1

[7] C. Barrett *et al.*, "Analysis problems for sequential dynamical systems and communicating state machines," in *Proc. of MFCS*. Springer, 2001, pp. 159–172. 1

[8] C. Kuhlman *et al.*, "Analysis problems for special classes of bi-threshold dynamical systems," in *Proc. Workshop on MAIN 2013*, 2013, pp. 26–33. 1

[9] C. Barrett *et al.*, "Predecessor existence problems for finite discrete dynamical systems," *Theoretical Computer Science*, vol. 386, no. 1-2, pp. 3–37, 2007. 1

[10] D. Laschov, M. Margaliot, and G. Even, "Observability of boolean networks: A graph-theoretic approach," *Automatica*, vol. 49, no. 8, pp. 2351–2362, 2013. 1

[11] C. Barrett *et al.*, "Gardens of eden and fixed points in sequential dynamical systems," *Discrete Mathematics & Theoretical Computer Science*, no. Proceedings, 2001. 1

[12] Mehrab, Zakaria *et al.*, "An agent-based framework to study forced migration: A case study of ukraine," *PNAS Nexus*, vol. 3, no. 3, pp. page–080, 2024. 2

[13] ——, "Network agency: An agent-based model of forced migration from ukraine," in *Proc. of AAMAS*, 2024, pp. 1372–1380. 2

[14] S. H. E. Abdelhamid *et al.*, "GDSCalc: A web-based application for evaluating discrete graph dynamical systems," *Plos One*, vol. 10, no. 8, pp. 1–24, 2015. 2, 4

[15] M. Granovetter, "Threshold models of collective behavior," *American J. Sociology*, vol. 83, no. 6, 1978. 2

[16] C. Barrett *et al.*, "Reachability problems for sequential dynamical systems with threshold functions," *Theoretical Computer Science*, vol. 295, no. 1-3, pp. 41–64, 2003. 2

[17] C. J. Kuhlman *et al.*, "Inhibiting diffusion of complex contagions in social networks: theoretical and experimental results," *Data Mining and Knowledge Discovery*, vol. 29, pp. 423–465, 2015. 2

[18] C. J. Kuhlman, "Generalizations of threshold graph dynamical systems," Ph.D. dissertation, Virginia Tech, 2013. 2, 3

[19] M. Hancock *et al.*, "Effect of peer influence and looting concerns on evacuation behavior during natural disasters," in *Proc. of the COMPLEX NETWORKS 2021 10*. Springer, 2022, pp. 377–389. 2

[20] C. J. Kuhlman *et al.*, "Natural disaster evacuation modeling: the dichotomy of fear of crime and social influence," *Social Network Analysis and Mining*, vol. 12, pp. 1–18, 2022. 2

[21] A. E. Biondo, A. Pluchino, and A. Rapisarda, "Return migration after brain drain: A simulation approach," arXiv preprint arXiv:1206.4280, 2012. 2

[22] I. Maidanik, "The forced migration from Ukraine after the full scale Russian invasion: Dynamics and decision making drivers," *European Societies*, vol. 26, no. 2, pp. 469–480, 2024. 2

[23] Z. Mehrab, L. Stundal, S. Venkatramanan, S. Swarup, B. Lewis, H. S. Mortveit, C. L. Barrett, A. Pandey, C. R. Wells, A. P. Galvani *et al.*, "An agent-based framework to study forced migration: A case study of ukraine," *PNAS Nexus*, vol. 3, no. 3, p. page:080, 2024. 2

[24] D. J. Watts and S. H. Strogatz, "Collective dynamics of 'small-world' networks," *Nature*, vol. 393, no. 6684, pp. 440–442, 1998. 3, 8

[25] A.-L. Barabási and R. Albert, "Emergence of scaling in random networks," *Science*, vol. 286, no. 5439, 1999. 3, 8

[26] A. Reinhart, "A review of self-exciting spatio-temporal point processes and their applications," *Statistical Science*, vol. 33, no. 3, pp. 299–318, 2018. 4, 6

[27] C. Brunsdon, J. Corcoran, and G. Higgs, "Visualising space and time in crime patterns: A comparison of methods," *Computers, Environment and Urban Systems*, vol. 31, no. 1, pp. 52–75, 2007. 4

[28] T. Nakaya and K. Yano, "Visualising crime clusters in a space-time cube: An exploratory data-analysis approach using space-time kernel density estimation and scan statistics," *Transactions in GIS*, vol. 14, no. 3, pp. 223–239, 2010. 4

[29] Y. Hu, F. Wang, C. Guin, and H. Zhu, "A spatio-temporal kernel density estimation framework for predictive crime hotspot mapping and evaluation," *Applied Geography*, vol. 99, pp. 89–97, 2018. 4

[30] A. Duval, "What is 0^0, and who decides, and why does it matter?" AMS Blogs, 2018. 5

[31] M. Hardy, "Both 0^0 and 0^1 are undefined?" Mathematics Stack Exchange, 2013. [Online]. Available: https://math.stackexchange.com/q/495141 5

[32] IOM, "Returns report — general population survey round 19 (january 2025)," 2025. [Online]. Available: https://dtm.iom.int/es/node/47956 5

[33] A. G. Hawkes, "Spectra of some self-exciting and mutually exciting point processes," *Biometrika*, vol. 58, no. 1, pp. 83–90, 1971. 6

[34] L. Lesage *et al.*, "Hawkes processes framework with a gamma density as excitation function: application to natural disasters for insurance," *Meth. Comput. Appl. Probab.*, vol. 24, no. 4, pp. 2509–2537, 2022. 6

[35] P. Erdos, A. Rényi *et al.*, "On the evolution of random graphs," *Publ. Math. Inst. Hungarian Acad. Sci.*, vol. 5, no. 1, pp. 17–60, 1960. 7, 9

[36] E. Marino, "The long history of environmental migration: Assessing vulnerability construction and obstacles to successful relocation in shishmaref, alaska," *Global Environmental Change*, vol. 22, no. 2, pp. 374–381, 2012. 9

[37] R. M. Buzard *et al.*, "Barrier island reconfiguration leads to rapid erosion and relocation of a rural alaska community," *Journal of Coastal Research*, vol. 39, no. 4, pp. 625–642, 2023. 9

[38] I. D. Correa and J. L. Gonzalez, "Coastal erosion and village relocation: a colombian case study," *Ocean & Coastal Management*, vol. 43, no. 1, pp. 51–64, 2000. 9

[39] R. Barbuti *et al.*, "Modelling population dynamics using grid systems," in *Proc. of Revised Selected Papers of the SEFM 2012*. Springer, 2014, pp. 172–189. 9

[40] J. M. Kleinberg, "Navigation in a small world," *Nature*, vol. 406, no. 6798, pp. 845–845, 2000. 9

[41] Z. Mehrab, S. S. Ravi *et al.*, "Agent-based Social Simulation of Spatiotemporal Process-triggered Graph Dynamical Systems - Technical Report," github.com/dmehrab06/STPGDS/blob/main/GDS-SP-WSC-full.pdf, 2025, bII Technical Report: #2025-9. 9

[42] M. Mitzenmacher and E. Upfal, *Probability and Computing*. Cambridge University Press, 2009. 11

[43] A. Bernabeu *et al.*, "Spatio-temporal hawkes point processes: A review," *Journal of Agricultural, Biological and Environmental Statistics*, pp. 1–31, 2024. 12